Journal of Alloys and Compounds 507 (2010) 508–512

Contents lists available at ScienceDirect

Journal of Alloys and Compounds

journal homepage: www.elsevier.com/locate/jallcom

Electrical characterization of Au/3C-SiC/*n*-Si/Al Schottky junction

G.S. Chung [a], K.S. Kim [a], F. Yakuphanoglu [b,*]

[a] School of Electrical Engineering, University of Ulsan, South Korea
[b] Physics Department, Faculty of Science, Firat University, 23169 Elazig, Turkey

ARTICLE INFO

Article history:
Received 21 April 2010
Received in revised form 30 July 2010
Accepted 4 August 2010
Available online 11 August 2010

Keywords:
3C-SiC diode
Schottky diode
Interfacial state density

ABSTRACT

High temperature silicon carbide Schottky diode was fabricated with Au deposited on poly 3C-SiC thin film grown on *n*-type Si(1 0 0) using atmospheric pressure chemical vapor deposition. The charge transport mechanism of the diode was studied in the temperature range of 300–550 K. The forward and reverse bias currents of the diode increase strongly with temperature and the diode shows a non-ideal behavior due to the series resistance and the interface states associated with 3C-SiC. The charge transport mechanism is a temperature activated process, in which, the electrons passes over of the low barriers and in turn, the diode has a large ideality factor. The electrical parameters of the Au/3C-SiC/*n*-Si/Al Schottky diode were explained on the basis of the thermionic emission theory with double Gaussian distribution of the barrier heights due to the barrier height inhomogeneities at metal/semiconductor interface. The interface state density of the diode was determined by the conductance–frequency method and it was of order of 9.18×10^{10} eV^{-1} cm^{-2}.

1. Introduction

The wide energy band gap, high thermal conductivity, large breakdown field, and high saturation velocity of silicon carbide (SiC) make this material an ideal choice for high temperature, high power, high voltage electron devices. Its chemical inertness, high melting point, extreme hardness, and high wear resistance make it possible to fabricate sensors and actuators capable of performing in harsh environments. These properties have garnered increased interests in the use of SiC in micro/nano-electromechanical systems (M/NEMS) technology [1,2]. Wide band-gap semiconductors have recently emerged as important materials because of possibility of usage in high frequency, high temperature and high power devices [3,4]. Among different single-phase ceramics like TiC, SiC, the cubic SiC has received much attention as a promising semiconductor [5] and it is a rapidly developing semiconductor material for power devices owing to its superior physical and chemical properties [6,7] and silicon carbide is well known as an attracting material for high power, high voltage and high frequency as well as high temperature microelectronics, due in part to its wide band gap, high thermal conductivity, high hardness [6], high wear resistance, low thermal expansion coefficient, good chemical resistance [8]. SiC is a very promising semiconductor due to its physical and electrical properties and it has excellent material properties, which makes it superior to Si in a wide range of applications. Outstanding properties of silicon carbide make it a promising material for manufacturing of many semiconductor devices [9]. SiC is an ideal material for manufacturing devices for use in power electronics, high temperature electronics and microwave communication [10].

Metal-silicon carbide (SiC) interfaces play very important roles in many high-performance devices in optoelectronic, high temperature, high frequency, and power applications. Currently, hexagonal SiC (4H- and 6H-) substrates fabricated by a sublimation method are commercially available. These substrates have small areas and are very expensive. It is difficult to obtain large area substrates by sublimation because a high temperature (2000 °C) is needed. However, since 3C (cubic)-SiC can be deposited with large areas at low temperatures, it has many advantages in micro-electromechanical system (MEMS) applications [11]. 3C-SiC heteroepitaxially grown on Si wafers is very suitable for the MEMS technology using high temperature, high power, high frequency and bio-electrical devices because the electron mobility of 3C-SiC is more excellent than its hexagonal SiC [11–14].

In this work, the current–voltage and capacitance–conductance–frequency characteristics of a silicon carbide Schottky diode fabricated with Au deposited on poly 3C-SiC thin film grown on *n*-type Si(1 0 0) using atmospheric pressure chemical vapor deposition have been investigated and obtained characteristics are used to the current-transport mechanism, in homogeneity in the barrier height, ideality factor and series resistance dependence of temperature.

2. Experimental

Poly 3C-SiC thin films were grown on *n*-type Si(1 0 0) substrates using Ar (5 slm: Standard Liter per Minute), H_2 (1 slm), and HMDS $\{Si_2(CH_3)_6\}$ (1 sccm: Stan-

* Corresponding author. Tel.: +90 424 2370000x3621; fax: +90 424 2330062.
E-mail addresses: fyhanoglu@firat.edu.tr, fyhan@hotmail.com (F. Yakuphanoglu).

0925-8388/$ – see front matter © 2010 Elsevier B.V. All rights reserved.
doi:10.1016/j.jallcom.2010.08.004

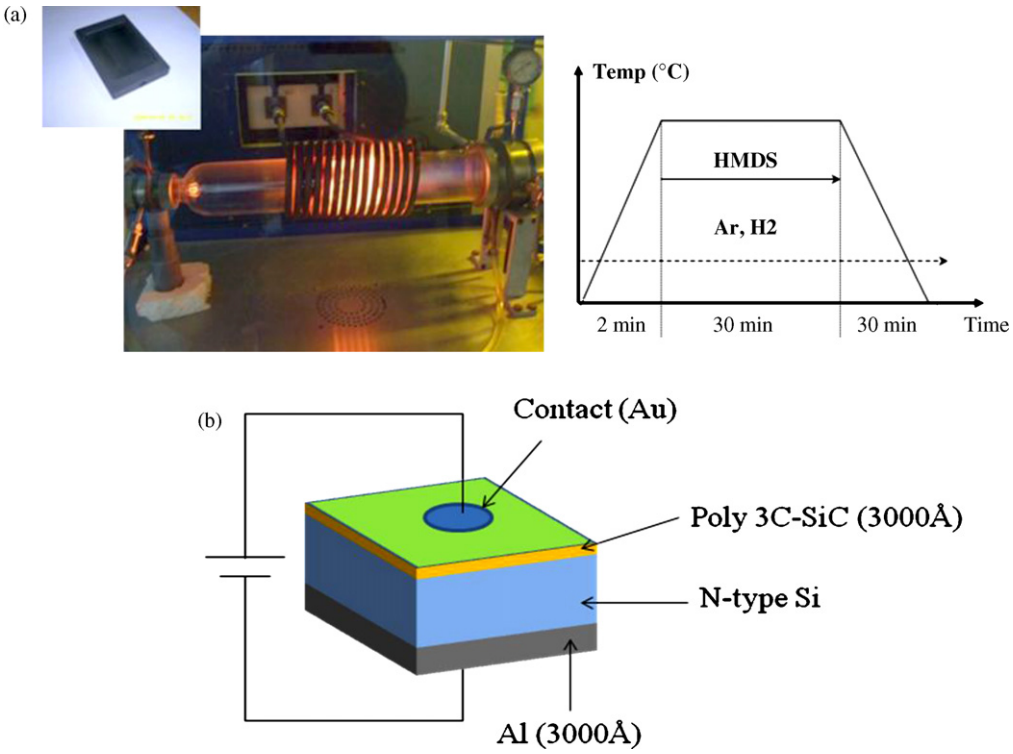

Fig. 1. (a) The reactor tube image of APCVD for the deposition of poly 3C-SiC thin film, (b) schematic structure of the diode.

dard Cubic Centimeter per Minute) gases by using APCVD (Atmospheric Pressure Chemical Vapor Deposition) for 30 min. Fig. 1(a) shows the optical image of APCVD and temperature profile [11]. The growth temperature and HMDS flow rate were 1200 °C and 8 sccm, respectively. The thickness of poly 3C-SiC was measured by AFM (Atomic Force Microscope and was found to be 3000 Å. The Schottky contact was fabricated with Au deposition on the surface of poly 3C-SiC by sputter. The circle Au diameter and thickness of the contact were 1 mm and 500 nm, respectively and thickness of Au contact was determined by thickness monitor. After deposition of Au, Al was deposited on the back side of Si substrate for ohmic contact. The contacts were achieved by vacuum annealing at 400 °C for 30 min. The schematic diagram of Au/3C-SiC/*n*-Si/Al Schottky diode is shown in Fig. 1(b). The current–voltage (*I*–*V*) characteristics of the Au/3C-SiC/*n*-Si/Al diode were performed with 2400 KEITHLEY source meter and GPIB data transfer card. The capacitance–voltage measurements were measured using a 3532 HIOKI HITESTER LCR. The temperature was controlled using a Lakeshore 331 S temperature controller.

3. Results and discussion

3.1. Current–voltage characteristics of Au/3C-SiC/n-Si/Al Schottky diode

The current–voltage characteristics of the Au/3C-SiC/*n*-Si/Al Schottky diode under various temperatures are shown in Fig. 2(a). The forward characteristics of the diode are linear in the semi-log scale. The forward and reverse currents of the diode increase strongly with temperature. This suggests that the temperature gives a significant effect on the carrier transport through Schottky contact. The increase in reverse bias current is higher than that of forward current of the diode. The diode shows a good rectifying behavior at investigated temperatures. The reverse saturation current of the diode changes with temperature. This is indicative of a change in the barrier height of the diode with increase of temperature. The *I*–*V* characteristics of the diode deviate from linearity due to the series resistance and the interface states associated with 3C-SiC. Thus, at lower voltages, the current–voltage characteristics of the diode can be expressed the following relation [15],

$$I = I_o \exp\left(\frac{q(V - IR_s)}{nkT}\right)\left[1 - \exp\left(-\frac{q(V - IR_s)}{kT}\right)\right] \quad (1)$$

where R_s is the series resistance, V is the applied voltage, n is the ideality factor, k is the Boltzmann constant, T is the temperature and I_o is the reverse saturation current.

At higher voltages, in order to analyze the charge transport mechanism, *I*–*V* characteristics of the diode were plotted in double logarithmic scale, as shown in Fig. 2b. The curves indicate two linear regions (regions I and II) obeying power law, $I = kV^m$ for the diode, here m is a exponent determining the charge transport mechanism. m values were calculated for both regions and were plotted, as shown in Fig. 2c. The obtained $m > 2$ values indicate that the charge transport mechanism at higher voltages is trap-filled space charge limited current (TCLC). As seen in Fig. 2c, the curves give a straight line, confirming that the charge transport mechanism is controlled by TCLC mechanism with an exponential trap.

The barrier height of the diode can be calculated by the following relation,

$$\phi_B = \frac{kT}{q} \ln\left(\frac{AA^*T^2}{I_o}\right) \quad (2)$$

where I_o is the saturation current, A is the contact area, A^* is the Richardson constant for 3C-SiC. The ϕ_B values were determined using I_o values obtained from ln *I*–*V* forward characteristics of the diode. The Richardson constant was calculated to be 81.6 A cm^{-2} K^{-2} using effective mass ($m^* = 0.68m_o$) [16]. For the determination of the barrier height, we can use of the Richardson plot given by the following relation

$$\ln\left(\frac{I_o}{T^2}\right) = -\frac{\phi_{Bo}}{kT} + \ln(A^*A) \quad (3)$$

Fig. 3 shows the plot of $\ln(I_o/T^2)$ vs $1/T$ for the diode. Fig. 3 was fitted by both linear and a non-linear fitting functions and the plot of $\ln(I_o/T^2)$ vs $1/T$ exhibits a non-linear behavior with $R^2 = 0.999$ value. This deviation in the Richardson plot indicates due to the presence of the spatially inhomogeneous BHs and potential fluctuations at the interface that consist of low- and high-barrier areas [17–20] and it will be later discussed in detail.

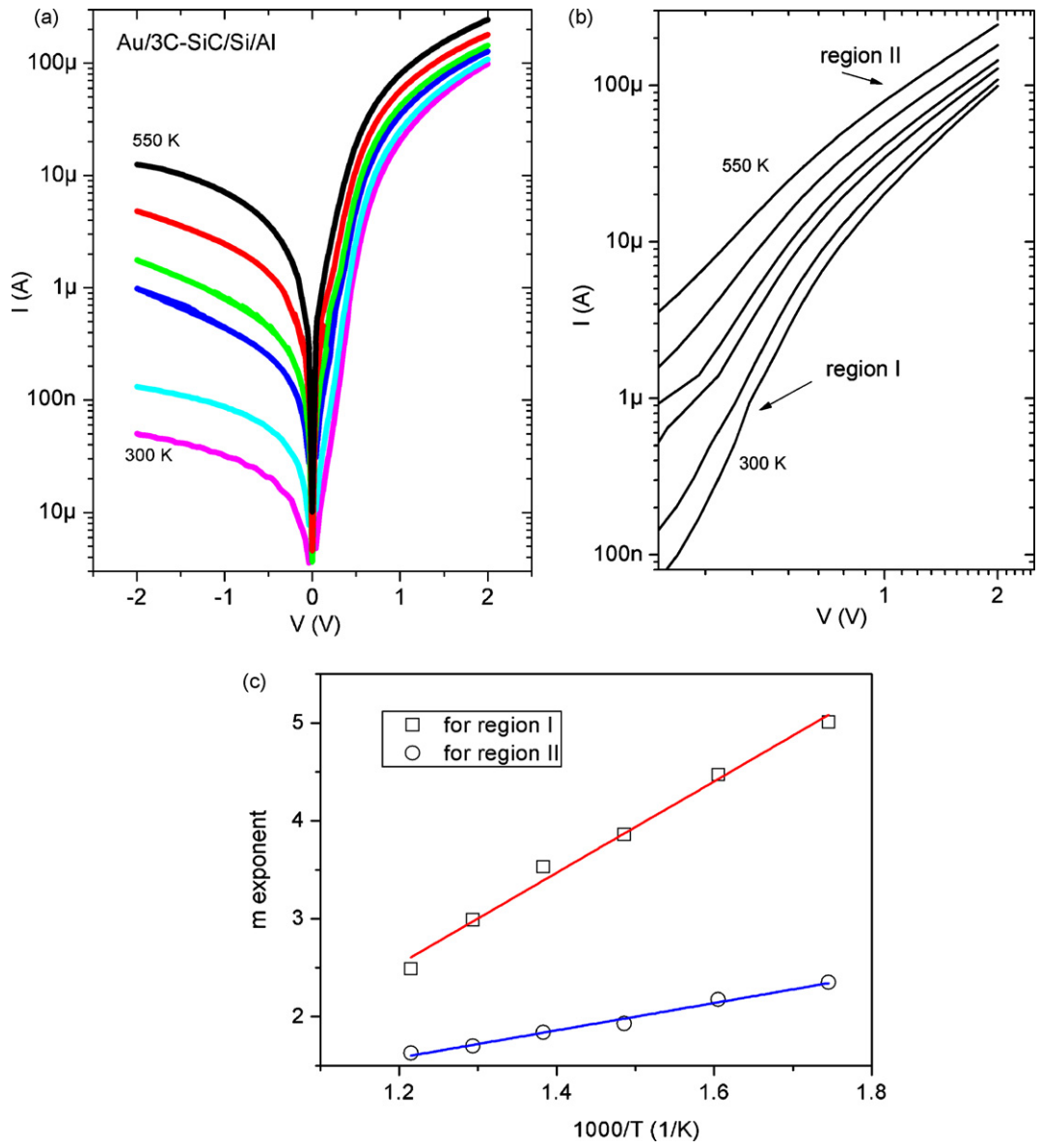

Fig. 2. (a) Current–voltage characteristics of the Au/3C-SiC/*n*-Si/Al diode at various temperatures with step of 50 K (b) *I–V* characteristics of the diode in double logarithmic scale (c) Plot of *m* vs 1000/*T* of the diode.

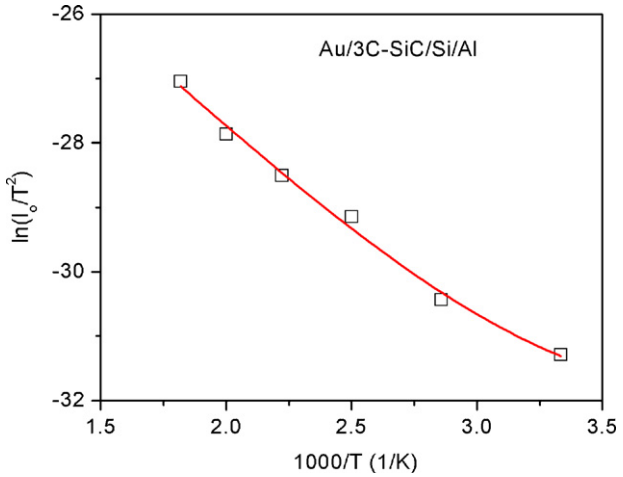

Fig. 3. Plot of $\ln(I_o/T^2)$ vs 1000/*T* of the Au/3C-SiC/*n*-Si/Al diode.

The series resistance is another important parameter on the current–voltage characteristics and in series resistance case, for determination of diode parameters, we can use Cheung's method defined by the following relations [21],

$$\frac{dV}{d\ \ln(I)} = n\frac{kT}{q} + IR_s \tag{4}$$

and

$$H(I) = V - n\frac{kT}{q}\ln\left(\frac{I_o}{AA^*T^2}\right) = IR_s + n\phi_B \tag{5}$$

where R_s is the series resistance and ϕ_B is the barrier height. The R_s, n and ϕ_B values were determined from plotted figures of $dV/d\ln I$ vs I and $H(I)$ vs I and are given in Table 1. The ideality factor of the diode decreases with increasing temperature, whereas the barrier height increases. The ideality factor obtained from the *I–V* characteristics is higher than unity and the higher ideality factor is affected by the high series resistance in the low Schottky barrier height patches. The current–voltage characteristics at various temperatures suggest that the charge transport mechanism is a

Table 1
Electrical parameters of the diode.

T (K)	n	R_s (Ω)	ϕ_B (eV)
300	2.97	1.70×10^4	0.79
350	2.91	1.49×10^4	0.89
400	2.78	1.11×10^4	0.98
450	2.51	9.71×10^3	1.09
500	2.39	7.79×10^3	1.18
550	2.15	5.92×10^3	1.28

temperature activated process, in which, the electrons passes over of the low barriers and in turn, the diode has a large ideality factor. The barrier height of the Au/3C-SiC/*n*-Si/Al diode for different temperatures was determined via Eq. (2). The decrease in barrier height and increase in the ideality factor with decreasing temperature are due to the discontinuities at the interface of the diode. The barrier height and ideality factor dependent on temperature are consistent with the presence of many low Schottky barrier height regions with Gaussian distribution at the interface [22]. As seen in Table 1, the R_s values of the diode are decreased with increase in temperature.

We can use the lateral distribution of barrier height if the barrier height has a Gaussian distribution. Gaussian distribution of the apparent barrier height and variation of the ideality factor with temperature are expressed by the following relations [22–25]

$$\phi_{ap} = \bar{\phi}_{bo} - \frac{q\sigma_o^2}{2kT} \tag{6}$$

and

$$\left(\frac{1}{n_{ap}} - 1\right) = \rho_2 - \frac{q\rho_3}{2kT} \tag{7}$$

where ϕ_{ap} is the apparent barrier height, σ_o is the standard deviation of the barrier height distribution, n_{ap} is the apparent ideality factor, ρ_2 and ρ_3 are voltage coefficients. The plots of $\phi_{ap} - 1/2kT$ and $1/n_{ap} - 1$ vs $1/2kT$ for the diode are shown in Fig. 4. These plots show two linear regions (I and II) and this confirms that two distributions are effective in the investigated temperature range [20,26]. Thus, the double Gaussian model is applied to temperature dependent distribution of the barrier height values region I in the temperature range of 300–400 K, and region II in the range of 400–550 K. The values of ρ_2 obtained from the intercept of the experimental n_{ap} vs $1/2kT$ plot are 0.283 in 400–550 K range and 0.576 in 300–400 K range, whereas the values of ρ_3 from the slopes are 0.0249 V in 400–550 K range and 0.00457 V in 300–400 K range. The values of $\bar{\phi}_{bo}$ and σ_o were determined from plot of $\phi_{ap} - 1/2kT$ and were found to be 2.06 eV and 0.27 V in the temperature range 400–550 K (the distribution 2), and 1.54 eV and 0.19 V in the temperature range 300–400 K (the distribution 1), respectively. The obtained barrier height values are dependent upon temperature and it is evaluated that two different current-transport mechanisms may dominate in measured temperature range. The barrier height inhomogeneities result from inhomogeneities in the composition of the interfacial insulator layer, nonhomogeneous of the interfacial charges and interfacial oxide layer thickness [25,26,22]. The standard deviation is a measure of the barrier inhomogeneity and more homogeneous barrier height is determined by lower value of σ_o. The obtained σ_o values confirm the barrier height inhomogeneities which arise from interfacial properties.

The reverse saturation current values of the diode increase with increase in temperature. This behavior can be analyzed using modified Richardson plot. The modified Richardson equation is expressed as follows [27]

$$\ln\left(\frac{I_o}{T^2}\right) - \left(\frac{q^2\sigma_o^2}{2k^2T^2}\right) = -\frac{\bar{\phi}_{bo}}{kT} + \ln(A^*A) \tag{8}$$

where $\bar{\phi}_{bo}$ is the zero-bias mean barrier height and I_o is the reverse saturation current. The plots of $\ln(I_o/T^2) - q^2\sigma_o^2/2K^2T^2$ vs $1000/T$ for distribution 1 and distribution 2 were plotted and are shown in Fig. 5. The $\bar{\phi}_{bo}$ and A^* values for the distribution 1 and distribution 2 were determined from the slope and intercept of Fig. 5 and were found to be 1.54 eV, 45.95 A cm^{-2} K^{-2} and 2.05 eV, 99.6 A cm^{-2} K^{-2}. The obtained A^* value for distribution 2 is close to obtained theoretically Richardson constant (81.6 A cm^{-2} K^{-2}). The values of $\bar{\phi}_{bo}$ for distribution 1 and distribution 2 are very close to obtained from plots of plot of $\phi_{ap} - 1/2kT$.

3.2. Interface state density properties of the Au/3C-SiC/n-Si/Al diode

The capacitance–frequency plots of Au/3C-SiC/*n*-Si/Al Schottky diode at different bias voltages are shown in Fig. 6. The capacitance increases with decreasing frequency due to a continuous distribution of the interface states. At lower frequencies, the capacitance of the diode has the higher values due to excess capacitance resulting from the interface states. At higher frequencies, the capacitance is not dispersive and the charges at the interface states cannot follow the fast alternating current signal and they do not contribute to the capacitance.

We have used the conductance technique described by Nicollian and Brews [28] to analyze interface state properties of Au/3C-SiC/*n*-Si/Al diode. It is well known that this method is most accurate method to evaluate the density of interface states. In the method, the parallel conductance is measured as a function of frequency at a

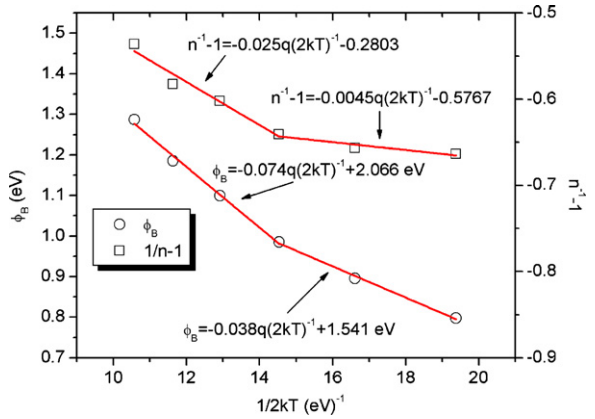

Fig. 4. Plots of ϕ_B and $n^{-1} - 1$ vs $1/2kT$ of the Au/3C-SiC/*n*-Si/Al diode.

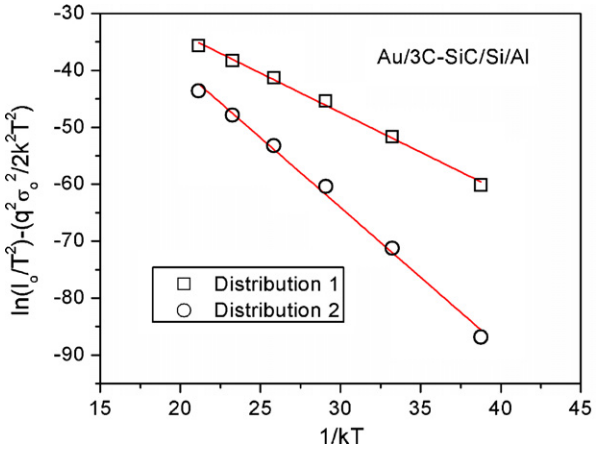

Fig. 5. Plot of $\ln(I_o/T^2) - q^2\sigma_o^2/2K^2T^2$ vs $1/kT$ of the Au/3C-SiC/*n*-Si/Al diode.

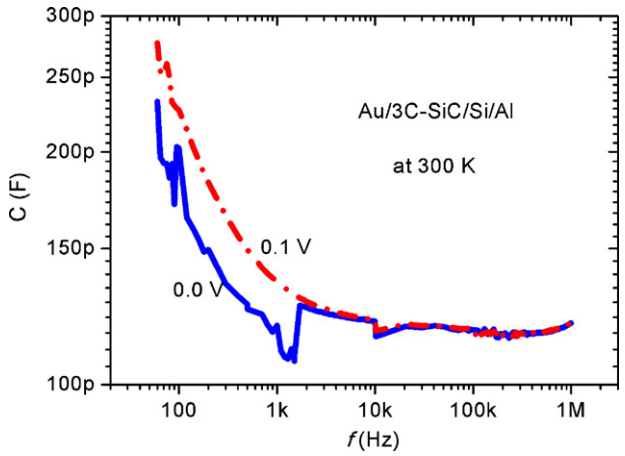

Fig. 6. Plots of C–f of the Au/3C-SiC/*n*-Si/Al diode at various voltages.

gate bias. In this method, C_p and G_p values are expressed as [28,29],

$$C_p = C_s + \frac{C_{it}}{1+(\omega\tau_{it})^2} \tag{9}$$

and

$$\frac{G_p}{\omega} = \frac{q\omega\tau_{it}D_{it}}{1+(\omega\tau_{it})^2} \tag{10}$$

where $C_{it} = qD_{it}$, $\tau_{it} = R_{it}C_{it}$ and τ_{it} is the interface trap constant. The normalized conductance is expressed as,

$$\frac{G_p}{\omega} = \frac{qAD_{it}\tau_{it}}{2\omega\tau_{it}}\ln(1+\omega^2\tau_{it}^2) \tag{11}$$

where D_{it} is the density of the interface states, q is the charge of the electron, ω is the angular frequency, τ is the time constant of the interface states. The relation between parallel conductance and measured capacitance-conductance is expressed as,

$$\frac{G_p}{\omega} = \frac{\omega G_m C_{ox}^2}{G_m^2 + \omega^2(C_{ox}-C_m)^2} \tag{12}$$

where C_{ox} is the capacitance of oxide layer. The maximum value of Eq. (10) is obtained taking $\left[d(G_p/\omega)/d(\ln\omega)\right] = 0$ and maximum condition is found to be $\omega\tau = 1.98$. This value is substituted into Eq. (10) and the interface state density is expressed as

$$D_{it} = \frac{(G/\omega)_{max}}{0.402qA} \tag{13}$$

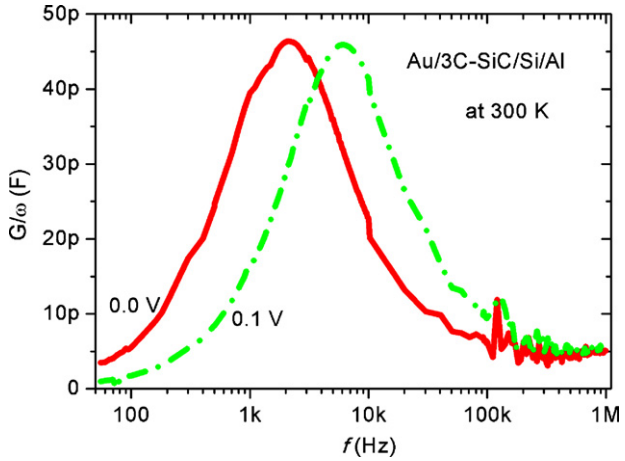

Fig. 7. Plots of G/ω – f of Au/3C-SiC/*n*-Si/Al diode at various voltages.

Fig. 7 shows the plots of $\ln(G/\omega)$ vs f of the diode at different voltages. The plots of $G_p/\omega - f$ indicate a peak. The origin of this peak is due to the presence of interface charges and these charges are present at interface of the silicon carbide-oxide layer, which are contributing to the total charging current and in turn a peak appears in the $G/\omega - f$ plot. The peak position shifts to higher frequencies with bias applied. This indicates that the traps are distributed inside the SiC band gap. The interface state density for the diode was of order of 9.18×10^{10} eV^{-1} cm^{-2}.

4. Conclusions

Gaussian distribution of inhomogeneous barrier height and determination of interface state density in Au/3C-SiC/*n*-Si/Al Schottky diode have been investigated by current–voltage and conductance–frequency methods. The ideality factor and barrier height values of the diode vary with temperature. The temperature dependent on ideality factor and barrier height was explained by on the basis of the thermionic emission with double Gaussian distribution of the barrier heights at the interface. The obtained standard deviation values of the barrier height distribution and mean barrier height values show the existence of interface inhomogeneties. The interface state density of the diode was found to be 9.18×10^{10} eV^{-1} cm^{-2}.

Acknowledgements

This research was supported by the Korea Research Foundation Grant through the Human Resource Training Project for Regional Innovation funded by 2010 the Korean Government which was conducted by the Ministry of Education, Science and Technology.

References

[1] P.M. Sarro, Sens. Actuators A 3 (2000) 210.
[2] K.-S. Kim, K.-B. Han, G.-S. Chung, Physica B 405 (2010) 513.
[3] K. Çınar, C. Coşkun, Ş. Aydoğan, H. Asıl, E. Gür, Nucl. Instrum. Methods Phys. Res., Sect. B 268 (2010) 616.
[4] L. Cao, H. Jiang, H. Song, Z. Li, G. Miao, J. Alloys Compd. 489 (2010) 562.
[5] B. Ghosh, S.K. Pradhan, J. Alloys Compd. 486 (2009) 480.
[6] J. Yi, X.D. He, Yue Sun, J. Alloys Compd. 491 (2010) 436.
[7] A.E. Bazin, J.F. Michaud, C. Autret-Lambert, F. Cayrel, T. Chassagne, M. Portail, M. Zielinski, E. Collard, D. Alquiera, Mater. Sci. Eng. B 171 (2010) 120.
[8] H. Zheng, Z. Fu, B. Lin, X. Li, J. Alloys Compd. 426 (2006) 290.
[9] M. Haberlen, J.W. Gerlach, B. Murphy, J.K.N. Lindner, B. Stritzker, J. Cryst. Growth 312 (2010) 762.
[10] L. Lianbi, C. Zhiming, L. Jia, Z. Yangyang, W. Jiannong, J. Lumin. 130 (2010) 587.
[11] G.S. Chung, J.H. Ahn, Microelec. Eng. 85 (2008) 1772.
[12] Q. Panga, L. Xu, Z. Ju, Z. Xing, L. Yang, Q. Hao, Y. Qian, J. Alloys Compd. 501 (2010) 60.
[13] J.-M. Liu, W.-Y. Chen, J. Hwang, C.-F. Huang, W.-L. Wang, L. Chang, Thin Solid Films 518 (2010) 5700.
[14] Y. Ikoma, R. Okuyama, M. Arita, T. Motooka, Thin Solid Films 518 (2010) 3759.
[15] E.H. Rhoderick, R.H. Williams, Metal–Semiconductor Contacts, Clarendon, Oxford, 1988.
[16] N.T. Son, O. Kordina, A.O. Konstantinov, W.M. Chen, E. Sorman, B. Monemar, E. Janzen, Appl. Phys. Lett. 65 (1994) 3209.
[17] M. Biber, A. Turut, J. Electron. Mater. 31 (2002) 1362.
[18] R.T. Tung, Phys. Rev. B 45 (1992) 13509.
[19] S. Huang, B. Shen, M.J. Wang, F.J. Xu, Y. Wang, H.Y. Yang, F. Lin, L. Lu, Z.P. Chen, Z.X. Qin, Z.J. Yang, G.Y. Zhang, Appl. Phys. Lett. 91 (2007) 072109.
[20] S. Demirezen, Ş. Altındal, Curr. Appl. Phys. 10 (2010) 1188.
[21] S.S.K. Cheung, N.W. Cheung, Appl. Phys. Lett. 49 (1986) 85.
[22] J.H. Werner, H.H. Güttler, J. Appl. Phys. 69 (1991) 1522.
[23] S. Chand, J. Kumar, J. Appl. Phys. 82 (1997) 5005.
[24] S. Zhu, R.L. VanMeirhaeghe, S. Forment, G. Ru, B. Li, Solid-State Electron. 48 (2004) 29.
[25] F.E. Cimilli, M. Sağlam, H. Efeoğlu, A. Türüt, Physica B 404 (2009) 1558.
[26] A. Tataroğlu, Ş. Altındal, J. Alloys Compd. 479 (2009) 893.
[27] M. Özer, D.E. Yıldız, Ş. Altındal, M.M. Bülbül, Solid-State Electron. 51 (2007) 941.
[28] E.H. Nicollian, A. Goetzberger, Appl. Phys. Lett. 7 (1965) 216.
[29] M.E. Aydin, F. Yakuphanoglu, Microelec. Eng. 85 (2008) 1836.